PROCEEDINGS OF SCIENCE

Characterizing Strongly Interacting Matter at Finite Temperature: (2+1)-Flavor QCD with Möbius Domain Wall fermions

Jishnu Goswami,[a,*] **Yasumichi Aoki,**[a] **Hidenori Fukaya,**[b] **Shoji Hashimoto,**[c,d] **Issaku Kanamori,**[a] **Takashi Kaneko,**[c,d,e] **Yoshifumi Nakamura**[a] **and Yu Zhang**[a] **(JLQCD collaboration)**

[a] *RIKEN Center for Computational Science (R-CCS),Kobe 650-0047, Japan*
[b] *Department of Physics, Osaka University, Toyonaka, Osaka 560-0043, Japan*
[c] *KEK Theory Center, High Energy Accelerator Research Organization (KEK), Tsukuba 305-0801, Japan*
[d] *School of High Energy Accelerator Science, Graduate University for Advanced Studied (SOKENDAI), Tsukuba 305-0801, Japan*
[e] *Kobayashi-Maskawa Institute for the Origin of Particles and the Universe, Nagoya University, Aichi, 464-8603, Japan*

E-mail: jishnu.goswami@riken.jp

In this proceeding, we present our ongoing calculations related to the thermodynamics of (2+1)-flavor Quantum Chromodynamics (QCD) using Möbius Domain Wall fermions. This report presents our findings on the second order quark number susceptibilities and conserved charge fluctuations. These calculations were performed on the line of constant physics (LCP), where the light quark mass m_l is set to 0.1 times the strange quark mass m_s. Additionally, we use the hadron resonance gas (HRG) model to compare against our results. This comparison is specific to temperatures at or below the pseudo-critical temperature, denoted as T_{pc}. We determine the pseudo-critical temperature from a preliminary analysis using the peak of the disconnected chiral susceptibility for the LCP with $m_l = 0.1m_s$ to be $T_{pc} = 165(2)$ MeV.

PREPRINT NUMBER: KEK-CP-0397

The 40th International Symposium on Lattice Field Theory (Lattice 2023)
July 31st - August 4th, 2023
Fermi National Accelerator Laboratory

*Speaker

PoS(LATTICE2023)187

1. Introduction

RHIC and LHC are two central experimental facilities for heavy ion collision (HIC) experiments. The collisions of heavy nuclei facilitate the creation of quark-gluon plasma (QGP), a distinct state of matter. Upon cooling, the QGP undergoes a transition to ordinary hadronic matter, and a freeze-out occurs during this cooling process.

Lattice QCD calculations near freeze-out can be directly confronted with HIC experimental data of conserved charge fluctuations. In heavy ion collisions, the three conserved charges are baryon number (B), electric charge (Q), and strangeness number (S). However, among them, only electric charge fluctuations are accessible in experiments, as detectors can measure almost all charged particles. Proton and kaon fluctuations are used as proxies for baryon number fluctuations and strangeness fluctuations, respectively [1].

However, calculations of electric charge fluctuations on the lattice pose computational challenges, as this observable is sensitive to the light pion spectrum in the hadronic phase. Pions are the pseudo-goldstone bosons of the spontaneous chiral symmetry $SU(2)_L \times SU(2)_R$ breaking, which explains their small mass. A lattice action with better chiral properties is required to get the correct pion spectrum on the finite lattice. For instance, in staggered fermion formalism, the taste symmetry violations can distort the pion spectrum, leading to large discretization errors in electric charge fluctuations. We use Möbius Domain Wall fermions [2], which are computationally expensive but have a better control on the chiral symmetry on the lattice. The pion spectrum will be intact at finite lattice spacing. Previous work on the study of the chiral phase transition on the line of constant physics (LCP) ($m_l = m_s/10$) using Möbius Domain Wall fermions is presented in [3, 4]. In this proceeding, we focus on quark number susceptibility and conserved charge fluctuations. In the following sections, all the dimensionful lattice parameters are expressed in lattice units, except otherwise stated explicitly. Previous exploratory work of quark number susceptibility using Domain wall fermions is found in [5], and free field theory calculations are in [6].

2. Lattice Setup

The gauge configurations for (2+1)-flavor QCD are generated using the Möbius Domain Wall fermions (MDWFs) and tree-level improved Symanzik gauge action, using the Rational hybrid Monte Carlo algorithm (RHMC) [3, 4]. The MDWFs Dirac operator is parameterized with $b = 1.5$, $c = 0.5$, $M_5 = 1$, where b and c are the Möbius parameters in the Möbius Domain Wall fermions Kernel, and M_5 is the mass parameter in the fifth dimension. The fifth dimension is set to a length of $L_s = 12$. Following [7], this parameter[1] choice, combined with three levels of stout-link smearing, effectively minimizes chiral symmetry violations.

In previous calculations, the lattice spacing a is determined as a function of gauge coupling β using the t_0 scale [3]. We perform all the simulations on a line of constant physics (LCP), i.e., as the temperature changes the bare quark masses have been adjusted such that the values of hadron masses in physical units, evaluated at zero temperature, stay approximately constant. We choose a

[1]The notation of the parameters we follow is summarized in the supplement material of [2], which is different from the one used in [7]

line of constant physics (LCP) as follows:

$$\frac{m_l}{m_s} = \frac{m_l^{latt}}{m_s^{latt}} = 0.1. \tag{1}$$

m_l and m_s are the light and strange quark mass respectively. And, m_f^{latt}, $(f = l, s)$ is the multiplicatively renormalizable mass. A strategy for determining the line of constant physics (LCP) with minimal zero-temperature simulations is outlined in [3]. However, due to the absence of zero temperature data at $\beta = 4.00$ the obtained $m_s(\beta)$ values were found to be smaller than the physical strange quark mass ($m_s^{phys} = 92.2(1)$ MeV) [8] for $\beta \leq 4.10$. Figure 1 (left) compares the old LCP (LCP2022) with the corrected LCP (LCP2023). We have performed simulations on two temporal extents, $N_\tau = 12$ where the β range is $4.00 \leq \beta \leq 4.17$ and $N_\tau = 16$ where the β range is $4.10 \leq \beta \leq 4.30$. Thus, on $N_\tau = 12$ lattices, the zero temperature hadron masses are expected to be smaller than those on $N_\tau = 16$ lattices.

Due to the finite L_s, one needs to take care of the residual mass m_{res}. As outlined in [3] the m_{res} is the same size as the error of m_s^{phys} while the size is comparable to the m_l^{phys}. The simulations are performed in two rounds. First, gauge configurations were generated for $N_\tau = 12, 16$ lattices for the LCP ($m_l = 0.1 m_s$), and measurements of m_{res}, chiral observables are performed. In the next round, the input quark masses for simulations are prepared by subtracting the m_{res}($m_f = m_f^{latt} - m_{res}$). Figure 1 (right) shows m_{res} as a function of β. For $N_\tau = 12$ lattices, within the β range of $4.00 \leq \beta \leq 4.17$, new gauge configurations were generated using $m_f = m_f^{latt} - m_{res}$, as m_{res} is the same size as m_l^{latt} and measurements are performed on these new configurations. For $N_\tau = 16$ lattices, where the β range is $4.10 \leq \beta \leq 4.30$ and m_{res} is significantly smaller than m_l^{latt}, we perform reweighting. It's noteworthy that m_{res} values are almost independent of the light quark mass (m_u^{latt}), suggesting that these m_{res} values can be used to tune input quark masses in simulations for the physical light quark masses.

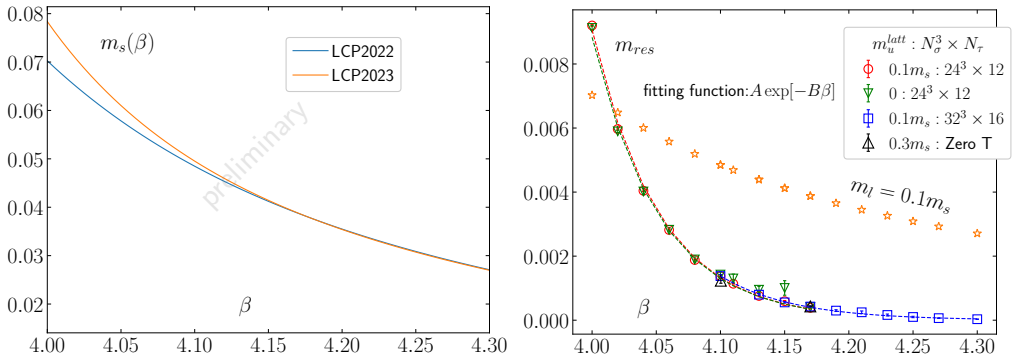

Figure 1: (left)$m_s(\beta)$ as a function of gauge coupling. (right) m_{res} and one tenth of the strange quark mass as a function of β.

N_σ	N_τ	#Config. per Temp.	N_n for $(D_1^f)^2$	N_n for D_2^f
24	12	~ 400	200	100
32	16	~ 200	200	100

Table 1: Details of the simulation parameters. N_σ and N_τ are spatial and temporal dimensions respectivley. N_n is the number of Gaussian random noise.

3. Quark Number Susceptibility with Möbius Domain Wall fermions

For two light flavors (u, d) and one strange flavor(s) in QCD, the pressure can be represented via a Taylor expansion in terms of the quark chemical potentials:

$$\frac{P}{T^4} = \frac{1}{VT^3} \ln Z(T, V, \vec{\mu}) = \sum_{i,j,k=0}^{\infty} \frac{\chi_{ijk}^{uds}}{i!j!k!} \hat{\mu}_u^i \hat{\mu}_d^j \hat{\mu}_s^k.$$
$$\chi_{ijk}^{uds} = \frac{1}{VT^3} \frac{\partial^{i+j+k} \ln Z(T, V, \vec{\mu})}{\partial \hat{\mu}_u^i \partial \hat{\mu}_d^j \partial \hat{\mu}_s^k}\bigg|_{\vec{\mu}=0}; \quad \text{provided } i+j+k \text{ is even.} \tag{2}$$

Here, $\hat{\mu}_f = \frac{\mu_f}{T}$ for $f \in \{u, d, s\}$ and $\vec{\mu} = (\mu_u, \mu_d, \mu_s)$. The coefficients χ_{ijk}^{uds} represent the quark number fluctuations at $\vec{\mu} = \vec{0}$: To implement the quark chemical potential into the Möbius

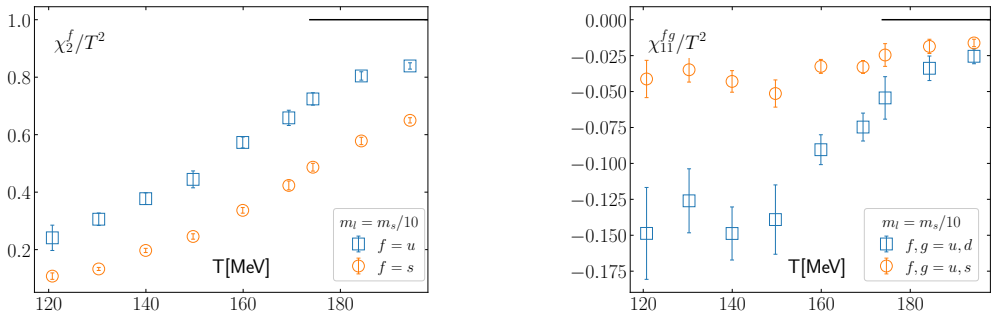

Figure 2: Diagonal (left) and Off-diagonal(right) quark number susceptibilities at the Line of constant physics ($m_l = m_s/10$) for the $24^3 \times 12 \times 12$. The black line represents the Boltzmann limit.

Domain Wall fermions action, we use the prescription $(1 \pm \gamma_4) U_{\pm 4}(x) \rightarrow (1 \pm \gamma_4) e^{\pm \hat{\mu}} U_{\pm 4}(x)$ [9, 10]. The partition function, Z, is defined as:

$$Z = \int DU \prod_{f=u,d,s} \det M(m_f, \mu_f) \exp[-S_g],$$
$$\det M(m_f, \mu_f) = \left[\frac{\det D(m_f, \mu_f)}{\det D(m_{PV}, \mu_f)} \right]. \tag{3}$$

The diagonal and off-diagonal quark number susceptibility for Möbius Domain Wall fermions

are defined as (with $m_{PV} \equiv 1$):[2]

$$\chi_2^f/T^2 = \frac{N_\tau}{N_\sigma^3}\frac{\partial^2 \ln Z}{\partial \hat{\mu}_f^2} = \left\langle \frac{\partial^2}{\partial \hat{\mu}_f^2} \ln\det M(m_f,\mu_f)\right\rangle + \left\langle \left(\frac{\partial}{\partial \hat{\mu}_f} \ln\det M(m_f,\mu_f)\right)^2\right\rangle \quad (4)$$

$$= \langle D_2^f \rangle + \langle (D_1^f)^2\rangle \quad (5)$$

$$\chi_{11}^{fg}/T^2 = \frac{N_\tau}{N_\sigma^3}\frac{\partial^2 \ln Z}{\partial \hat{\mu}_f \hat{\mu}_g} = \left\langle \left(\frac{\partial}{\partial \hat{\mu}_f} \ln\det M(m_f,\mu_f)\right)\left(\frac{\partial}{\partial \hat{\mu}_g} \ln\det M(m_g,\mu_g)\right)\right\rangle \quad (6)$$

$$= \langle D_1^f D_1^g\rangle \quad (7)$$

$(D_1^f)^2$ is the most noisy part in our calculations. We have used 200 Gaussian random sources for estimating $(D_1^f)^2$ and 100 Gaussian random sources for estimating D_2^f, see in Table1. We utilize spin dilution and time slice dilution (see appendix) to calculate $(D_1^f)^2$ using the unbiased estimator method. Moreover, we have utilized the Even-Odd dilution method to calculate D_2^f.

Fig. 2 represents the quark number susceptibilities as a function of temperature computed using Möbius Domain Wall fermions in (2+1)-flavor QCD along the line of constant physics ($m_l = 0.1m_s$). The value of these susceptibilities stays small at smaller temperatures and they start a rapid change near the pseudo-critical temperature ($T_{pc} \sim 165(2)$ MeV) and approach an asymptotic value at higher temperatures ($T \sim 190$ MeV). These results are qualitatively consistent with those from staggered discretization for physical quark masses [11, 12]. In the next section, we will use these quark number susceptibilities and construct conserved charge fluctuations.

4. Conserved charge fluctuations with Möbius Domain Wall fermions

We present all the second-order fluctuations of conserved charges using the relation between baryon (μ_B), electric charge (μ_Q), and strangeness (μ_S) chemical potentials and the quark chemical potentials as [11]:

$$\mu_u = \frac{1}{3}\mu_B + \frac{2}{3}\mu_Q, \quad \mu_d = \frac{1}{3}\mu_B - \frac{1}{3}\mu_Q, \quad \mu_s = \frac{1}{3}\mu_B - \frac{1}{3}\mu_Q - \mu_S. \quad (8)$$

Second-order conserved charge fluctuations can be written as:

$$\begin{pmatrix} \chi_2^B \\ \chi_2^Q \\ \chi_2^S \\ \chi_{11}^{BQ} \\ \chi_{11}^{QS} \\ \chi_{11}^{BS} \end{pmatrix} = \begin{pmatrix} \frac{1}{9}(2\chi_2^u + \chi_2^s + 2\chi_{11}^{ud} + 4\chi_{11}^{us}) \\ \frac{1}{9}(5\chi_2^u + \chi_2^s - 4\chi_{11}^{ud} - 2\chi_{11}^{us}) \\ \chi_2^s \\ \frac{1}{9}(\chi_2^u - \chi_2^s + \chi_{11}^{ud} - \chi_{11}^{us}) \\ \frac{1}{3}(\chi_2^s - \chi_{11}^{us}) \\ -\frac{1}{3}(\chi_2^s + 2\chi_{11}^{us}) \end{pmatrix} \quad (9)$$

[2]Here, we simplify the notation by omitting the index if its value is zero, e.g., $\chi_{200}^{uds} \equiv \chi_2^u$, $\chi_{110}^{uds} \equiv \chi_{11}^{ud}$, and $\chi_{101}^{uds} \equiv \chi_{11}^{us}$.

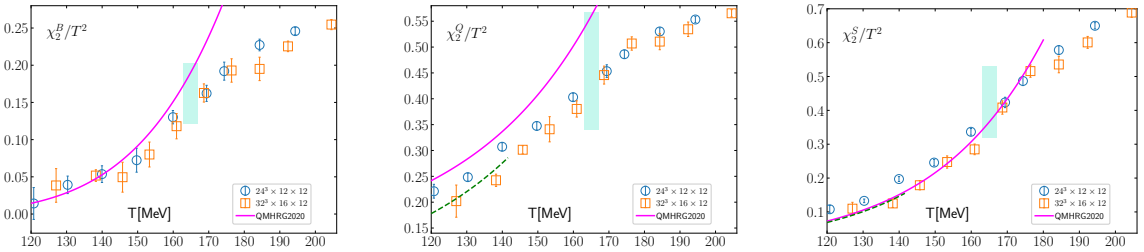

Figure 3: Diagonal second order fluctuations as a function of temperature at the line of constant physics ($m_l = 0.1m_s$). The dashed line is the HRG calculations after modifying the $M_\pi \sim 223$ MeV and $M_K \sim 508$ MeV in the QMHRG2020 [13] list. The band represents the pseudo-critical temperature obtained from the peak of disconnected chiral susceptibility as shown in the appendix B.

4.1 Diagonal Second Order Fluctuations

Figure 3 presents the diagonal conserved charge fluctuations observed using MDWF fermions in $(2+1)$-flavor QCD for $N_\tau = 12, 16$, which are compared with QMHRG2020 results [13, 14]. At lower temperatures, the fluctuations shown in Figure 3 are explained by hadronic degrees of freedom. In the HRG model, the largest contributions to χ_2^B, χ_2^Q, and χ_2^S come from nucleons, pions, and kaons, respectively, at lower temperatures. For $m_l = 0.1m_s$, the hadron masses are larger than their physical values. Consequently, the values from HRG calculations using these larger masses will be slightly smaller than those calculated with the physical spectrum. The differences in χ_2^Q between lattice data and QMHRG2020 can be attributed to our slightly heavier light quark masses. The heavier light quark mass results in $M_\pi \sim 223$ MeV and $M_K \sim 508$ MeV, from the leading-order chiral perturbation theory. This means that compared to their physical counterparts, the pions and kaons in our simulations are heavier by approximately 60% and 2%, respectively. Furthermore, physical pions are three times lighter than physical kaons. Therefore, we observed that χ_2^Q is sensitive to the heavier ground state pion and kaon mass, as shown by the (green) dashed line in Figure 3. However, the effect on χ_2^S due to the change in ground state kaon mass is less pronounced. Given that nucleons are significantly heavier than pions and kaons, it is anticipated that the QMHRG2020 curves for χ_2^B will be slightly smaller and consistent with our lattice data.

Moreover, at least a part of the difference between the $N_\tau = 12$ and $N_\tau = 16$ data for χ_2^Q can be understood from HRG arguments. As shown in Figure 1 (left), the mistuning of the LCP results in smaller pion and kaon masses on the $N_\tau = 12$ lattice than the $M_\pi \sim 223$ MeV and $M_K \sim 508$ MeV, which are obtained for $N_\tau = 16$ lattices. Therefore, a part of the observed differences in χ_2^Q in two different temporal extents can be attributed to the mistuning of the LCP.

4.2 Off-Diagonal Second Order Fluctuations

Figure 4 presents off-diagonal conserved charge fluctuations using MDWF fermions in $(2+1)$-flavor QCD, alongside comparisons with QMHRG2020 [13, 14]. In the HRG framework, χ_{11}^{BQ}, χ_{11}^{QS}, and χ_{11}^{BS} are dominated by charged nucleons, charged kaons, and strange baryons, respectively. As discussed in the previous section, it is expected that the HRG values for these fluctuations will also be slightly reduced and are consistent with the lattice data.

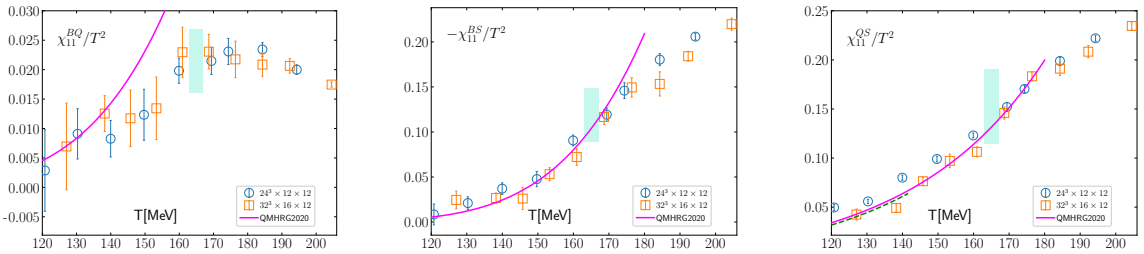

Figure 4: Off-diagonal second order fluctuations as a function of temperature at the Line of constant physics ($m_l = 0.1m_s$). The dashed line is the HRG calculations after modifying the $M_\pi \sim 223.5$ MeV and $M_K \sim 508.4$ MeV in the QMHRG2020 [13] list. The blue band represents the pseudo-critical temperature obtained from the peak of disconnected chiral susceptibility[4].

5. Summary and outlook

We present the quark number susceptibility and all the second-order conserved charge fluctuations for (2+1)-flavor Quantum Chromodynamics (QCD) using Möbius Domain Wall fermions. These simulations are performed along the line of constant physics (LCP), where the light quark mass m_l is 0.1 times the strange quark mass m_s. We compare our calculations with those from the Hadron Resonance Gas (HRG) model with the QMHRG2020 particles list. We argue that second-order conserved fluctuations are consistent with the HRG model with heavier hadrons at temperatures below T_{pc}. Moreover, we argue that electric charge fluctuations are particularly sensitive to the ground state pion and kaon mass at low temperatures. As part of our ongoing research, we are extending these simulations with physical values for the light quark masses.

Acknowledgements

The project is supported by the MEXT as “Program for Promoting Researches on the Supercomputer Fugaku” (JPMXP1020200105),“Simulation for basic science: approaching the quantum era" (JPMXP1020230411) and Joint Institute for Computational Fundamental Science (JICFuS). I. K. acknowledges JPS KAKENHI (JP20K0396). The simulations are performed on the supercomputer “Fugaku” at RIKEN Center for Computational Science (HPCI project hp230207,hp200130, hp210165, hp220174 and Usability Research ra000001). We used the Grid [15, 16] for configuration generations and Bridge++ [17–19] for measurements. We use AnalysisToolbox [20, 21] for statistical data analysis. We thank the JLQCD collaboration members for fruitful discussions. J.G. also thank Frithjof Karsch and Christian Schmidt for discussions on conserved charge fluctuations.

References

[1] M. Asakawa and M. Kitazawa, *Fluctuations of conserved charges in relativistic heavy ion collisions: An introduction*, *Prog. Part. Nucl. Phys.* **90** (2016) 299 [1512.05038].

[2] JLQCD collaboration, *Form factors of $B \to \pi \ell \nu$ and a determination of $|Vub|$ with Möbius domain-wall fermions*, *Phys. Rev. D* **106** (2022) 054502 [2203.04938].

[3] Y. Aoki, S. Aoki, H. Fukaya, S. Hashimoto, I. Kanamori, T. Kaneko et al., *2+1 flavor fine lattice simulation at finite temperature with domain-wall fermions*, *PoS* **LATTICE2021** (2022) 609 [2112.11771].

[4] S. Aoki, Y. Aoki, H. Fukaya, J. Goswami, S. Hashimoto, I. Kanamori et al., *Thermodynamics with Möbius domain wall fermions near physical point II*, *PoS* **LATTICE2022** (2023) 176 [2303.05884].

[5] M. Cheng, N. H. Christ, M. Li, R. D. Mawhinney, D. Renfrew, P. Hegde et al., *The finite temperature QCD using 2 + 1 flavors of domain wall fermions at N (t) = 8*, *Phys. Rev. D* **81** (2010) 054510 [0911.3450].

[6] R. V. Gavai and S. Sharma, *Thermodynamics of free Domain Wall fermions*, *Phys. Rev. D* **79** (2009) 074502 [0811.3026].

[7] S. Hashimoto, S. Aoki, G. Cossu, H. Fukaya, T. Kaneko, J. Noaki et al., *Residual mass in five-dimensional fermion formulations*, *PoS* **LATTICE2013** (2014) 431.

[8] Flavour Lattice Averaging Group (FLAG) collaboration, *FLAG Review 2021*, *Eur. Phys. J. C* **82** (2022) 869 [2111.09849].

[9] J. C. R. Bloch and T. Wettig, *Domain-wall and overlap fermions at nonzero quark chemical potential*, *Phys. Rev. D* **76** (2007) 114511 [0709.4630].

[10] R. C. Brower, H. Neff and K. Orginos, *The Möbius domain wall fermion algorithm*, *Comput. Phys. Commun.* **220** (2017) 1 [1206.5214].

[11] S. Borsanyi, Z. Fodor, S. D. Katz, S. Krieg, C. Ratti and K. Szabo, *Fluctuations of conserved charges at finite temperature from lattice QCD*, *JHEP* **01** (2012) 138 [1112.4416].

[12] A. Bazavov et al., *The chiral and deconfinement aspects of the QCD transition*, *Phys. Rev. D* **85** (2012) 054503 [1111.1710].

[13] D. Bollweg, J. Goswami, O. Kaczmarek, F. Karsch, S. Mukherjee, P. Petreczky et al., *Second order cumulants of conserved charge fluctuations revisited: Vanishing chemical potentials*, *Phys. Rev. D* **104** (2021) [2107.10011].

[14] J. Goswami, F. Karsch, C. Schmidt, S. Mukherjee and P. Petreczky, *Comparing conserved charge fluctuations from lattice QCD to HRG model calculations*, *Acta Phys. Polon. Supp.* **14** (2021) 251 [2011.02812].

[15] P. Boyle, A. Yamaguchi, G. Cossu and A. Portelli, *Grid: A next generation data parallel C++ QCD library*, 1512.03487.

[16] P. Boyle, "Grid: Data parallel c++ mathematical object library." https://github.com/paboyle/Grid.

[17] S. Ueda, S. Aoki, T. Aoyama, K. Kanaya, H. Matsufuru, S. Motoki et al., *Development of an object oriented lattice QCD code 'Bridge++'*, *J. Phys. Conf. Ser.* **523** (2014) 012046.

[18] T. Aoyama, I. Kanamori, K. Kanaya, H. Matsufuru and Y. Namekawa, *Bridge++ 2.0: Benchmark results on supercomputer Fugaku*, *PoS* **LATTICE2022** (2023) 284 [2303.05883].

[19] "Lattice qcd code bridge++." http://bridge.kek.jp/Lattice-code/, 30 June 2023.

[20] L. Altenkort, D. A. Clarke, J. Goswami and H. Sandmeyer, *Streamlined data analysis in Python*, in *40th International Symposium on Lattice Field Theory*, 8, 2023, 2308.06652.

[21] D. A. Clarke et al., "Analysistoolbox." https://github.com/LatticeQCD/AnalysisToolbox.

[22] QCDSF collaboration, *Disconnected contributions to D-meson semi-leptonic decay form factors*, *PoS* **LATTICE2011** (2011) 283 [1111.4053].

Appendix

A. Stochastic error reduction in trace calculations

To evaluate the traces we employ stochastic trace estimators,

$$D_1^f = TrD(m_f)^{-1}\frac{dD}{d\mu_f} - TrD(m_{PV})^{-1}\frac{dD}{d\mu_f} \tag{10}$$

$$= \frac{1}{N_n}\sum_j^{N_n}\left[\eta_j^\dagger D(m_f)^{-1}\frac{dD}{d\mu_f}\eta_j - \eta_j^\dagger D(m_{PV})^{-1}\frac{dD}{d\mu_f}\eta_j\right] \tag{11}$$

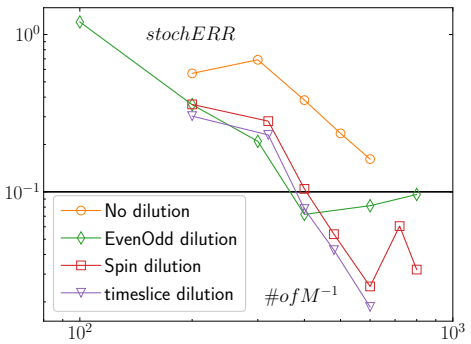

Figure 5: Stochastic error of $(D_1^f)^2$ with the number M^{-1}.

Where η_j is the Gaussian random noise vector and N_n is the total number of noise vectors. We have found that to decrease the stochastic error in $(D_1^f)^2$ useful to use identical noise vectors for both the flavor part and the Pauli-Villars part, as shown in Eq.(11). Below we will discuss how to further reduce the stochastic error using the dilution method.

A.1 Dilution

The dilution refers to dividing the single random noise vector into N components, with only one component assigned nonzero values at any given time. Then the trace measurement formula can be written as,

$$TrD(m)^{-1}\frac{dD}{d\mu_f} = \frac{1}{N_n}\sum_j^{N_n}\sum_{a=1}^{N}\eta_{aj}^\dagger D(m)^{-1}\frac{dD}{d\mu_f}\eta_{aj} \tag{12}$$

Where, m can be both m_f and m_{pv}. We explore three possibilities of the dilution,

1. **Even-Odd splitting of the noise vector**: This method splits the single noise vector into two parts ($N = 2$) in even and odd lattice sites.

2. **Spin partition**: The approach involves splitting the noise vector into four spin components ($N = 4$) and retaining non-zero values in only one spin component at a time [22].

3. **Time slice dilution** We employ a splitting technique for the noise vector based on a modulo 4 operation, $t \mod 4$. This method allows us to divide the noise vector into four distinct components, corresponding to different time slices.

The dilution method will also increase the number of inverses of the Dirac operator. Hence, in Fig.5 we compare the stochastic error for a single gauge configuration with the number of inverses and see that indeed the dilution method can reduce the stochastic error $2-3$ times. The spin dilution and the time slice dilution are the two most cost-effective methods. We use spin dilution for the $N_\tau = 12$ lattices and time slice dilution for the $N_\tau = 16$ lattices.

B. Determination of pseudo-critical temperature T_{pc} using chiral observables

In Figure 6 we show the disconnected chiral susceptibility (χ_{disc}) in the $\overline{MS}$ scheme for the LCP $m_l = 0.1m_s$. We show the results for the temporal extents of $N_\tau = 12$ with aspect ratios $N_\sigma/N_\tau = 2, 3, 4$ and $N_\tau = 16$ with the aspect ratio $N_\sigma/N_\tau = 2$. The value of pseudo-critical temperature (T_{pc}) is obtained from a preliminary analysis and using the peak of the susceptibilities for different lattice spacings and volumes. Despite the mismatch of the LCP, the discretization effects between $N_\tau = 12$ and $N_\tau = 16$ are smaller, and the peak of the χ_{disc} results in a consistent pseudo-critical temperature determination. Moreover, for the $N_\tau = 12$ lattice, where we have 3 aspect ratios, we extrapolate the T_{pc} to the $V \to \infty$ limit. In particular, from our preliminary analysis, we obtained $T_{pc} = 165(2)$ MeV. This pseudo-critical temperature, however, is not unique and it will depend on the observable.

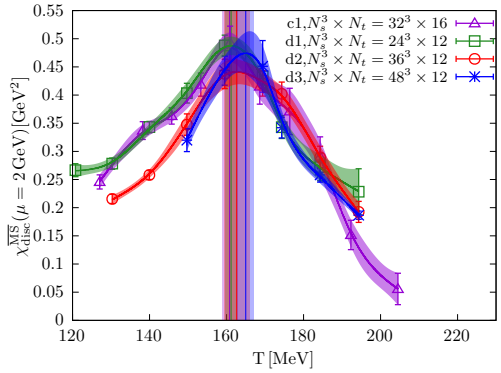

Figure 6: Disconnected chiral susceptibility for the LCP $m_l = 0.1m_s$.